Ecotoxicology and Environmental Safety 202 (2020) 110834

Contents lists available at ScienceDirect

Ecotoxicology and Environmental Safety

journal homepage: www.elsevier.com/locate/ecoenv

# A novel pathophysiological classification of silicosis models provides some new insights into the progression of the disease

Zhujie Cao[a,1], Meiyue Song[b,c,d,1], Ying Liu[a,1], Junling Pang[a], Zhaoguo Li[e], Xianmei Qi[a], Ting Shu[a], Baicun Li[a], Dong Wei[f], Jingyu Chen[f], Bolun Li[a], Jing Wang[a,*], Chen Wang[a,c,d,**]

[a] State Key Laboratory of Medical Molecular Biology, Institute of Basic Medical Sciences, Chinese Academy of Medical Sciences, Department of Pathophysiology, Peking Union Medical College, Beijing, China
[b] Beijing University of Chinese Medicine, Beijing, China
[c] Department of Pulmonary and Critical Care Medicine, Center of Respiratory Medicine, China-Japan Friendship Hospital, Beijing, China
[d] National Clinical Research Center for Respiratory Diseases, Beijing, China
[e] Department of Respiratory, The Second Affiliated Hospital of Harbin Medical University, Harbin, Heilongjiang, China
[f] The Affiliated Wuxi People's Hospital of Nanjing Medical University, Wuxi, China

ARTICLE INFO

*Keywords:*
Silicosis
Classification
Progression
Lung function
Pulmonary inflammation
Pulmonary fibrosis

ABSTRACT

Silicosis is caused by massive inhalation of silica-based particles, which leads to pulmonary inflammation, pulmonary fibrosis and lung dysfunction. Currently, the pathophysiological process of silicosis has not been well studied. Here, we defined the progression of silicosis as four stages by unsupervised clustering analysis: normal stage, inflammatory stage, progressive stage and fibrotic stage. Specifically, in normal stage, the lung function was normal, and no inflammation or fibrosis was detected in the lung tissue. Inflammatory stage showed a remarkable pulmonary inflammation but mild fibrosis and lung dysfunction. In progressive stage, significant lung dysfunction was observed, while pulmonary inflammation and fibrosis continued to deteriorate. Fibrotic stage revealed the most severe pulmonary fibrosis and lung dysfunction but no significant deterioration in inflammation. Since the common features were founded in both silicosis patients and rodents, we speculated that the pathophysiological processes of silicosis in patients might be similar to the rodents. Collectively, our new classification identified the process of silicosis, clarified the pathophysiological features of each stage, and provided some new insights for the progression of the disease.

## 1. Introduction

Silicosis is caused by occupational exposure to silica and is one of the leading occupational diseases worldwide (James SL et al., 2018). Although efforts to reduce silica exposure have been made for many decades, millions of workers are still exposed to silica worldwide, especially in developing countries (Cohen et al., 2016; James SL et al., 2018). The diagnosis of silicosis is based on occupational history and radiologic findings (Fernández et al., 2015; Muszyńska-Graca et al., 2016), but X-ray is not suitable for detecting early silicosis (Ehrlich et al., 2018). What's more, currently, there is no effective treatment to silicosis and lung transplantation remains the only option for patients with terminal silicosis (Joubert et al., 2019; Leung et al., 2012).

The main characters of silicosis include the aggravation of pulmonary inflammation, fibrosis and lung dysfunction. It has been reported that the number of leukocytes (macrophages, neutrophils and lymphocytes) and pro-inflammatory cytokines such as tumor necrosis factor-alpha (TNF-α), interleukin-1β (IL-1β), interleukin-6 (IL-6) in bronchoalveolar lavage fluid (BALF) are increased significantly in silicosis patients and rodents (Fujimura, 2000; Karkale et al., 2018; Leung et al., 2012; Vanhée et al., 1995; Zhai et al., 2004). Furthermore, fibrotic proteins such as collagen I and fibronectin are up-regulated in the silicosis lung tissues (Feng et al., 2020). In addition, lung function test, especially spirometry test, is the most common strategy to evaluate lung function in clinic (Leung et al., 2012). For example, FEV1 (forced expiratory volume in 1 s), FVC (forced vital capacity) or the ratio of FEV1/FVC can reflect the restrictive or obstructive ventilation disorders of the lung. Similarly, in silicosis rodents, the corresponding parameters such as forced expiratory volume 0.3s (FEV 300), static compliance (Crs), elastic resistance (Ers) and tissue elasticity (H) can also reveal the

* Corresponding author. No.5 Dongdansantiao Street, Dongcheng District, Beijing, PR China.
** Corresponding author. No.5 Dongdansantiao Street, Dongcheng District, Beijing, PR China.
*E-mail addresses:* wangjing@ibms.pumc.edu.cn (J. Wang), wangchen@pumc.edu.cn (C. Wang).
[1] Authors contributed equally.

https://doi.org/10.1016/j.ecoenv.2020.110834
Received 26 March 2020; Received in revised form 27 May 2020; Accepted 30 May 2020
Available online 01 July 2020

alteration of lung function in the progression of silicosis (Devos et al., 2017; Sun et al., 2019).

In the study of silicosis, the lack of a standardized animal model in different pathophysiological stages has become an obstacle. Most previous studies focused on the period of severe pulmonary fibrosis. However, during the progression of silicosis, no significant pulmonary fibrosis was found in the early stage (Zhao et al., 2020). Moreover, no unified protocol (various doses and exposure time of silica) was used to induce silicosis by intratracheal instillation. Specifically, the exposure time of 50 mg silica varies from weeks to months in rats (Fröhlich and Salar-Behzadi, 2014; Guo et al., 2019; Yan et al., 2016; Zhang et al., 2018). In mice, different exposure patterns were performed such as 1 mg of silica for 4 weeks, or 20 mg of silica for 2 weeks (Beamer et al., 2010; Cruz et al., 2016; Du et al., 2019; Kato et al., 2017; Mayeux et al., 2019). Therefore, establishing an appropriate animal model for different pathophysiological stages of silicosis is necessary to further explore molecular mechanisms, search diagnostic markers or screen drugs.

In this study, we classified the progression of silicosis into different stages and characterized the pathophysiological features of the disease. We first determined the important parameters that can be used to assess the progression of silicosis in human. Next, we established silicosis models using intratracheal instillation with different silica dose and exposure times on rodents and detected the alterations of these important parameters including lung function, right ventricular function, pulmonary inflammation and fibrosis. Finally, based on these data, silicosis models were classified into four clusters by unsupervised clustering analysis, and the pathophysiological features of each cluster were described. According to the different characteristics of each cluster, we defined the progression of silicosis as normal stage (cluster 1), inflammatory stage (cluster 2), progressive stage (cluster 3) and fibrotic stage (cluster 4).

## 2. Materials and methods

### 2.1. Human lung samples

Human lung tissue samples, including normal individuals (n = 5) and silicosis patients (n = 5), were obtained from Wuxi People's Hospital. These lung tissues came from discarded tissues of donors and recipients during lung transplantation operation, and organ donors agreed to organ donation. All experiments with human samples were performed under protocols approved by the Institutional Review Boards at Institute of Basic Medical Sciences, Chinese Academy of Medical Sciences, and Wuxi People's Hospital.

### 2.2. Crystalline silica

Crystalline silica (CAS7631-86-9; average particle diameter 1.6 μm; purity 99%) was purchased from Forsman Scientific (Beijing, China) Co., Ltd. Particulates were made endotoxin-free by baking at 200 °C for 2 h and were suspended in sterile phosphate-buffered saline (PBS). Suspensions were sonicated for 10 min before use.

### 2.3. Rat silicosis models

Male specific pathogen-free Wistar rats (200 ± 20 g, 8–10 weeks old) were purchased from the Vital River Laboratory Animal Technology Co. Ltd. (Beijing, China). The rats were kept in sterilized cages in rooms at 60–70% humidity and 24–26 °C with a 12/12 h dark–light cycle and given fresh water and food each week. And the animal room maintained specific pathogen-free conditions. Intratracheal instillation of silica (50 mg/mL, 1 mL) was used to induce silicosis in rats. In detail, the rats were placed on a platform and then anesthetized with an intraperitoneal injection of 2% pentobarbital (0.2 mL/100 g). Next, the trachea of rats was separated and silica suspension (50 mg/mL, 1 mL) was slowly added to the trachea with syringe. The control rats (Silica 0 mg) were injected with an equal amount of PBS solution. These rats were divided into eight groups (5 rats per group) according to the different silica exposure doses and times: 5 days (Silica 0 mg, Silica 50 mg), 10 days (Silica 0 mg, Silica 50 mg), 15 days (Silica 0 mg, Silica 50 mg) and 30 days (Silica 0 mg, Silica 50 mg). All experimental procedures were approved by the Animal Care and Use Committee of Peking Union Medical College.

### 2.4. Mouse silicosis models

C57BL/6 J male mice (25 ± 2 g, 8–10 weeks old) were purchased from the Vital River Laboratory Animal Technology Co. Ltd. (Beijing, China). The feeding conditions of mice were same as rats. The similar method was used to induce silicosis in mice. However, unlike rats, the mice were intratracheally instilled at different doses including: 4 mg (200 mg/mL, 20 μL), 8 mg (400 mg/mL, 20 μL), 12 mg (600 mg/mL, 20 μL) and 16 mg (800 mg/mL, 20 μL). According to the different exposure doses and time, mice were divided into fifteen groups (5 mice per group): 3 weeks groups (0 mg, 4 mg, 8 mg, 12 mg, 16 mg), 6 weeks groups (0 mg, 4 mg, 8 mg, 12 mg, 16 mg), and 9 weeks groups (0 mg, 4 mg, 8 mg, 12 mg 16 mg). All experimental procedures were approved by the Animal Care and Use Committee of Peking Union Medical College.

### 2.5. Lung function test

Forced Pulmonary Maneuver System was used to test lung function of rats (Buxco® Research Systems, Data Sciences International (DSI), St. Paul, MN 55112 U.S.A.). And lung function of mice was tested by a computer-controlled ventilator (FlexiVent, SCIREQ, Montreal, Quebec, Canada). See the Supplementary materials for the detailed process of lung function test of rats and mice.

### 2.6. Hemodynamic measurement

Right ventricular systolic pressures (RVSP) in rats and mice were tested by an eight-gauge disposable venous infusion needle connected to a pressure transducer and Power Lab Data Acquisition and Analysis System (PL 3504, AD Instruments, Australia). Briefly, after blunt separation of the left anterior thoracic muscles, the needle was inserted into the right ventricle of anesthetized rats and mice. RVSP was recorded by Power Lab and analyzed using Lab Chart 8 software.

### 2.7. Right ventricular hypertrophy index measurement

The right ventricles, left ventricles and septa were separated after the hearts were removed. The right ventricular hypertrophy index (RVHI) was obtained by calculating the ratio of right ventricular (RV) weight to the sum of left ventricular (LV) and septal (S) weight (RV/[LV + S]).

### 2.8. Histological staining and analysis

Hematoxylin-eosin (HE) staining, Masson staining and Sirius red staining were performed in the lung tissues of human, rats and mice. See the Supplementary materials for the details.

### 2.9. Hydroxyproline assay

The contents of hydroxyproline (HYP) in the lung tissues were measured by the Hydroxyproline Assay Kit (NBP2-59,747, Novus Biologicals, Littleton, CO, USA) according to the manufacturer's instructions. The absorbance of the sample was measured at 560 nm, and converted to HYP concentration in μg/mL.

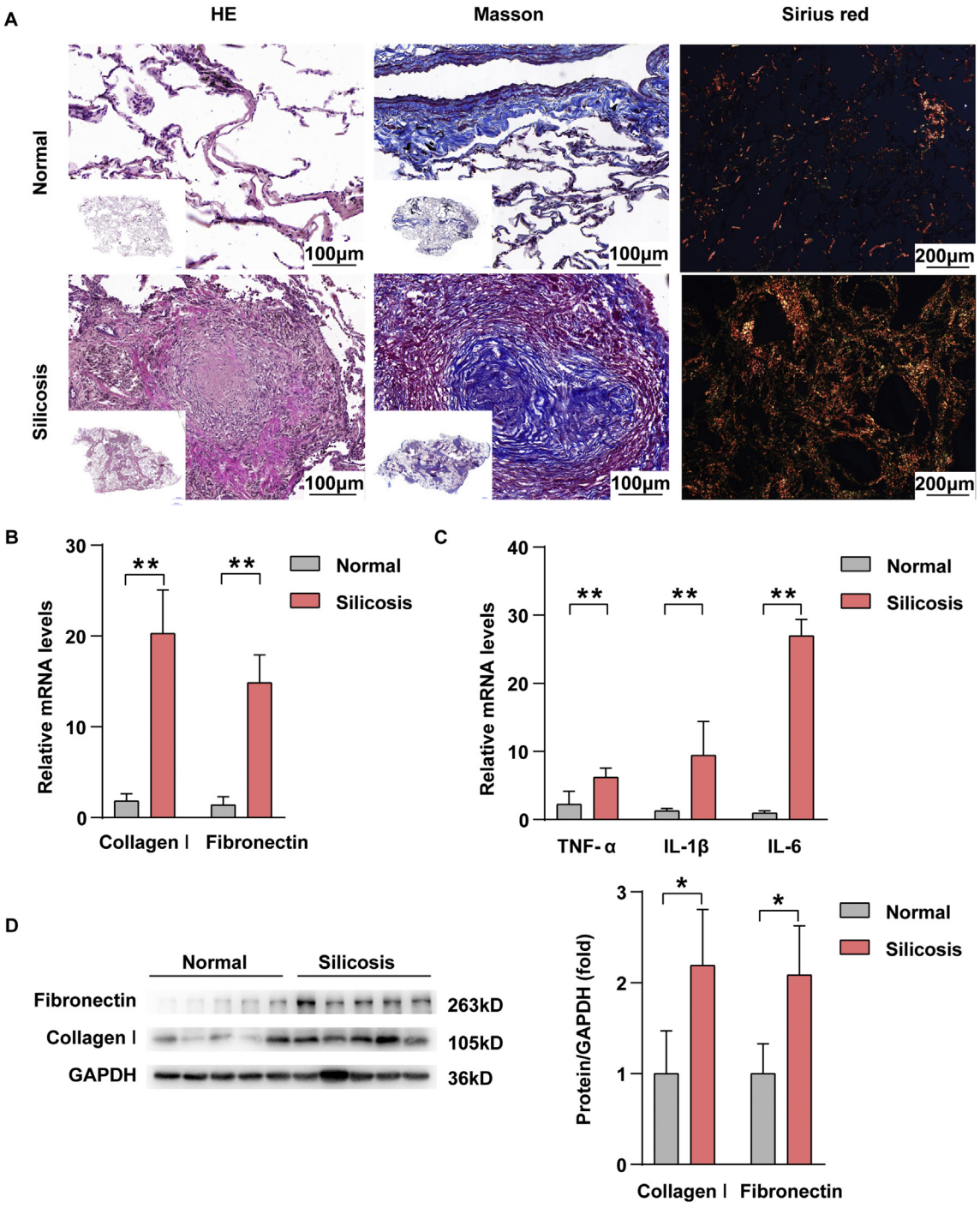


**Fig. 1.** Identify the pathophysiological characteristics of lung tissues in silicosis patients. A, HE staining, Masson staining and Sirius red staining were performed in lung tissues of normal individuals and silicosis patients (n = 5 for each group). B, mRNA expression of collagen I and fibronectin in lung tissue from normal individuals and silicosis patients was detected by qPCR (n = 5 for each group). C, mRNA expression of TNF-α, IL1β and IL6 in lung tissues from normal individuals and silicosis patients was detected by qPCR (n = 5 for each group). D, Western blot showed the protein expression of collagen I and fibronectin in lung tissues from normal individuals and silicosis patients (n = 5 for each group). For all statistical plots, the data are presented as the mean ± SD; $^{*}P < 0.05$; $^{**}P < 0.01$. (For interpretation of the references to colour in this figure legend, the reader is referred to the Web version of this article.)

### *2.10. Leucocyte counts in BALF*

Bronchoalveolar lavage (BAL) was performed to collect leukocytes from the bronchial and alveolar space. See the Supplementary materials for the specific experimental process.

### *2.11. ELISA*

The supernatants of bronchoalveolar lavage fluid (BALF) from rats and mice were detected by enzyme-linked immunosorbent assay (ELISA) kits according to the manufacturer's instructions. See the Supplementary Material Table 4 for specific kit information.

**Table 1**
Parameters of lung function and right ventricle function in different rat silicosis models.

| Rat silicosis models[c] | 5 Days | | 10 Days | | 15 Days | | 30 Days | |
|---|---|---|---|---|---|---|---|---|
| | Silica 0 mg | Silica 50 mg | Silica 0 mg | Silica 50 mg | Silica 0 mg | Silica 50 mg | Silica 0 mg | Silica 50 mg |
| RVHI (%) | 24.42 ± 2.09 | 30.88 ± 2.21[b] | 24.33 ± 2.48 | 31.4 ± 2.35[b] | 26.93 ± 1.87 | 32.94 ± 2.66[b] | 29.33 ± 3.42 | 30.68 ± 2.11 |
| RVSP (mmHg) | 20.35 ± 2.03 | 22.19 ± 1.92 | 20.46 ± 2.03 | 22 ± 2.09 | 20.82 ± 2.34 | 22.55 ± 2.01 | 21.22 ± 2.37 | 26.85 ± 1.33[b] |
| Rl ($cmH_2O$*secs/mL) | 0.3 ± 0.03 | 0.3 ± 0.02 | 0.31 ± 0.03 | 0.31 ± 0.03 | 0.32 ± 0.03 | 0.38 ± 0.05[a] | 0.32 ± 0.03 | 0.46 ± 0.05[b] |
| Cdyn (mL/cm $H_2O$) | 0.19 ± 0.03 | 0.31 ± 0.03[b] | 0.24 ± 0.03 | 0.25 ± 0.01 | 0.25 ± 0.04 | 0.21 ± 0.02 | 0.24 ± 0.03 | 0.2 ± 0.03[b] |
| IC (mL) | 11.1 ± 1.07 | 10.77 ± 1.52 | 11.28 ± 0.96 | 9.69 ± 0.91 | 11.68 ± 1.4 | 9.38 ± 1.71[b] | 11.51 ± 1.51 | 8.04 ± 0.7[b] |
| FVC (mL) | 14.23 ± 1.32 | 13.67 ± 2.17 | 14.46 ± 1.34 | 12.13 ± 1.18[a] | 14.97 ± 1.83 | 12.37 ± 1.16[a] | 14.75 ± 1.47 | 9.73 ± 1.85[b] |
| Cfvc50 (mL/cm $H_2O$) | 1 ± 0.1 | 0.78 ± 0.08[b] | 1.01 ± 0.11 | 0.75 ± 0.09[b] | 1.05 ± 0.12 | 0.69 ± 0.07[b] | 1.03 ± 0.11 | 0.69 ± 0.12[b] |
| FRC (mL) | 3.35 ± 0.31 | 3.42 ± 0.63 | 3.41 ± 0.31 | 3.37 ± 0.48 | 3.53 ± 0.42 | 3.33 ± 0.27 | 3.47 ± 0.31 | 3.5 ± 0.35 |
| Cchord (mL/cm $H_2O$) | 0.6 ± 0.06 | 0.54 ± 0.05 | 0.61 ± 0.06 | 0.5 ± 0.24 | 0.63 ± 0.08 | 0.47 ± 0.1[a] | 0.62 ± 0.06 | 0.3 ± 0.05[b] |
| FEV300 (mL) | 13.7 ± 1.38 | 16.35 ± 1.53[a] | 13.93 ± 1.31 | 11.49 ± 1.09[a] | 14.41 ± 1.71 | 13.07 ± 1.91 | 14.21 ± 1.5 | 9.03 ± 1.81[b] |
| MMEF (mL/sec) | 80.71 ± 8.03 | 96.31 ± 11.77[a] | 82.05 ± 8.12 | 85.8 ± 8.12 | 84.92 ± 10.42 | 74.24 ± 8.21 | 83.72 ± 10.02 | 65.07 ± 7.47[b] |

Values are mean ± SD.
[a] $P < 0.05$, [b] $P < 0.01$. Silica 50 mg versus Silica 0 mg in 5 days, 10 days, 15days and 30 days respectively.
Abbreviations: RVHI, right ventricular hypertrophy index; RVSP, right ventricular systolic pressure; Rl, lung resistance; Cdyn, dynamic compliance; IC, inspiratory capacity; FVC, forced vital capacity; Cfvc50, compliance at 50% vital capacity; FRC, functional residual capacity; Cchord, quasi-static compliance; FEV300, forced expiratory volume in the first 300 ms of expiration; MMEF, mean mid expiratory flow.
[c] Rats were exposed to single dose (50 mg) and different exposure time (5 days, 10 days, 15 days and 30 days) of silica, lung tissue and BALF were collected at 5 days, 10 days, 15days and 30 days respectively.

### 2.12. Quantitative real-time PCR

TRIzol reagent (Invitrogen, Carlsbad, CA, USA) was used to extract total messenger RNA (mRNA) from lung tissues. mRNA was reverse-transcribed into complementary DNA (cDNA) using a Tiangen kit (KR103, Tiangen Biotechnology, Beijing, China). SYBR Green I Q-PCR kit (TransGen Biotech, Beijing, China) was used to amplify cDNA in a Bio-Rad IQ5 system (Bio-Rad, Hercules, CA, USA). The expression of mRNA was normalized to β-actin expression, and the primers used in this experiment were listed in the Supplementary Material Table 5.

### 2.13. Western blot analysis

Total protein samples were extracted from lung tissues by RIPA lysis buffer (P0013b, Beyotime, Shanghai, China). BCA Protein Assay Kit (23,225, Thermo Fisher Scientific, Waltham, MA, USA) was used to detect the concentration of protein samples. The protein samples (20 μg) were separated on an 8% SDS–polyacrylamide gel electrophoresis gel, transferred to a polyvinylidene fluoride membrane, incubated overnight at 4 °C with specific primary antibodies, then incubated with specific secondary antibodies at room temperature for 1 h. The protein signal was detected by Tanon Automatic Chemiluminescence/Fluorescence Image Analysis System (5200, Tanon, Shanghai, China), and GAPDH served as the control. See the Supplementary Material Table 6 for specific antibodies information.

### 2.14. Statistical analysis

Data were analyzed using SPSS (version 20.0) software and were expressed as the mean ± SD. Two-way analysis of variance (ANOVA) was used to evaluate the effects of silica dose and silica exposure time on various parameters of mice. Two-tailed Student's *t*-test was used to analyze the differences among two groups in human and rats. One-way ANOVA was used to analyze the differences among clusters in both rats and mice. $P < 0.05$ was considered statistically significant.

Unsupervised clustering analysis was performed for all the samples with various clinical variables using a hierarchical clustering algorithm (hclust). The distance matrix was obtained with the "euclidean" method, while the clustering method was used with "ward.D". The values of clinical variables were scaled among samples when clustering. Four super clusters of the samples were highlighted based on the clustering results. The clustering analysis and the generation of diagrams were conducted with the "pheatmap package" (version 1.0.12) (https://cran.r-project.org/web/packages/pheatmap/index.html) in R (version 3.4.3).

## 3. Results

### 3.1. Identify the pathophysiological characteristics of lung tissues in silicosis patients

To define the appropriate parameters to reveal the pathophysiological progression of silicosis, we selected the parameters (TNF-α, IL-1β, IL-6, collagen I and fibronectin) that have been reported in rodent silicosis models and examined these parameters in lung tissues from normal individuals and silicosis patients with severe pulmonary fibrosis. As shown in Fig. 1A, HE staining of silicosis patients showed a severe bronchoalveolitis with numerous of leukocytes around the bronchial and alveolar interstitial compared to normal individuals (Fig. 1A). Consistently, inflammatory cytokines (TNF-α, IL-1β, IL-6) were significantly up-regulated in lung tissues of silicosis patients (Fig. 1C). In addition, Masson staining revealed severe pulmonary fibrosis in silicosis lung tissues indicated by typical silicotic nodules with collagen fibers arranging in concentric circles (Fig. 1A). And birefringent collagen I/III (red or green, respectively) were observed under polarized light microscopy by Sirius red staining (Fig. 1A). Consistently, fibrotic markers (collagen I and fibronectin) were also increased in the lung tissues of silicosis patients at both mRNA and protein levels (Fig. 1B and D). Taken together, our results suggested that these parameters (TNF-α, IL-1β, IL-6, collagen I and fibronectin) can be used to reflect the general progress of silicosis in both human and rodents. Moreover, these results also identified some pathophysiological characteristics of pulmonary inflammation and fibrosis in silicosis patients.

### 3.2. Clarify the pathophysiological characteristics of silicosis in different rat models

To determine the pathophysiological characteristics of silicosis in different rat models, we detected the important parameters including lung function, right ventricular function, pulmonary inflammation and fibrosis in rats with different silica exposure times. As Table 1 shown, silica exposure impaired lung function in a time-dependent manner, which was characterized by a disturbance in pulmonary ventilation mode, as well as lung compliance and resistance. Specifically, lung function test showed a restrictive ventilatory disorder in the medium

**Table 2**
Parameters of pulmonary inflammation and pulmonary fibrosis in different rat silicosis models.

| Rat silicosis models | 5 Days | | 10 Days | | 15 Days | | 30 Days | |
|---|---|---|---|---|---|---|---|---|
| | Silica 0 mg | Silica 50 mg | Silica 0 mg | Silica 50 mg | Silica 0 mg | Silica 50 mg | Silica 0 mg | Silica 50 mg |
| Inflammatory parameters | | | | | | | | |
| Szapiel scores_HE stain | 0 ± 0 | 1 ± 0[b] | 0 ± 0 | 1.2 ± 0.45[b] | 0 ± 0 | 2.4 ± 0.55[b] | 0 ± 0 | 2.8 ± 0.45[b] |
| Macrophage counts ($10^7$/L)_BALF | 1.23 ± 0.08 | 6.15 ± 0.34[b] | 1.01 ± 0.09 | 7.01 ± 0.43[b] | 1.16 ± 0.2 | 13.78 ± 1.31[b] | 1.43 ± 0.24 | 13.6 ± 3.41[b] |
| Lymphocyte counts ($10^7$/L)_BALF | 0.01 ± 0 | 0.11 ± 0.03 | 0.02 ± 0.01 | 0.52 ± 0.43[b] | 0.02 ± 0.02 | 0.6 ± 0.39[b] | 0.03 ± 0.02 | 0.8 ± 0.38[b] |
| Neutrophil counts ($10^7$/L)_BALF | 0.23 ± 0.03 | 1.11 ± 0.15 | 0.34 ± 0.07 | 1.97 ± 0.36[a] | 0.02 ± 0.01 | 11.04 ± 3.23[b] | 0.05 ± 0.04 | 6.24 ± 1.14[b] |
| TNF-α (pg/mL)_BALF | 13.98 ± 1.98 | 18.28 ± 0.6[b] | 12.21 ± 0.73 | 20.93 ± 1.62[b] | 12.16 ± 1.08 | 23.44 ± 1.11[b] | 12.38 ± 1.08 | 27.28 ± 1.7[b] |
| IL1β (pg/mL)_BALF | 38.83 ± 1.62 | 42.89 ± 1.34[a] | 37.95 ± 0.66 | 56.37 ± 2.51[b] | 37.66 ± 2.7 | 63.34 ± 1.72[b] | 35.91 ± 2.86 | 73.24 ± 5.99[b] |
| IL6 (pg/mL)_BALF | 40.4 ± 2.14 | 56.87 ± 2.45[b] | 35.79 ± 1.15 | 64.36 ± 1.26[b] | 37.05 ± 2.71 | 72.97 ± 3.03[b] | 38.08 ± 2.46 | 87.57 ± 4.7[b] |
| TNF-α _mRNA (relative levels) | 1.16 ± 0.43 | 3.22 ± 1.29[a] | 1.48 ± 0.65 | 4.83 ± 1.47[b] | 1.38 ± 0.42 | 5.7 ± 2.57[b] | 1.17 ± 0.29 | 6.25 ± 0.62[b] |
| IL1β _mRNA (relative levels) | 1.03 ± 0.27 | 1.1 ± 0.39 | 1.12 ± 0.13 | 1.02 ± 0.48 | 1.13 ± 0.32 | 1.75 ± 0.12[b] | 1.31 ± 0.33 | 2.14 ± 0.44[b] |
| IL6 _mRNA (relative levels) | 0.91 ± 0.1 | 6.23 ± 2.78[b] | 0.87 ± 0.27 | 3.96 ± 0.73[a] | 1.2 ± 0.24 | 12.62 ± 2.3[b] | 1.4 ± 0.54 | 12.46 ± 4.69[b] |
| Fibrotic parameters | | | | | | | | |
| Fibrotic scores_ Masson stain | 0.13 ± 0.04 | 2.26 ± 1.09 | 0.13 ± 0.04 | 9.21 ± 2.23 | 0.13 ± 0.04 | 11.56 ± 5.25 | 0.13 ± 0.04 | 88.88 ± 34.86[b] |
| Sirius red staining positive area | 71.95 ± 8.24 | 455.79 ± 78.66 | 72.02 ± 7.64 | 2048.48 ± 438.01[b] | 73.14 ± 7.79 | 5277.66 ± 175.74[b] | 67.71 ± 4.62 | 7157.01 ± 1043.1[b] |
| HYP (μg/mg wet lung) | 2.08 ± 0.08 | 2.26 ± 0.13[a] | 2.11 ± 0.09 | 2.77 ± 0.08[b] | 2.02 ± 0.08 | 3.27 ± 0.11[b] | 2.11 ± 0.09 | 3.63 ± 0.17[b] |
| COL-I_protein (fold) | 1 ± 0.16 | 1.69 ± 0.38[b] | 1 ± 0.22 | 2.33 ± 0.52[b] | 1 ± 0.18 | 2.62 ± 0.12[b] | 1 ± 0.24 | 2.82 ± 0.1[b] |
| FN _protein (fold) | 1 ± 0.41 | 1.41 ± 0.58 | 1 ± 0.34 | 2.06 ± 0.52[b] | 1 ± 0.27 | 2.28 ± 0.33[b] | 1 ± 0.14 | 3.47 ± 0.25[b] |
| COL-I_mRNA (relative levels) | 1.12 ± 0.29 | 2.19 ± 0.39[a] | 1.44 ± 0.4 | 6.28 ± 1.08[b] | 1.25 ± 0.54 | 9.99 ± 0.38[b] | 1.45 ± 0.58 | 14.92 ± 0.91[b] |
| FN _mRNA (relative levels) | 1.04 ± 0.1 | 1.54 ± 0.16 | 1.01 ± 0.37 | 1.92 ± 0.32[a] | 1.3 ± 0.29 | 2.8 ± 0.48[b] | 1.65 ± 0.54 | 4.45 ± 1.36[b] |

Values are mean ± SD.
[a] $P < 0.05$, [b] $P < 0.01$. Silica 50 mg versus Silica 0 mg in 5 days, 10 days, 15days and 30 days respectively.
Abbreviations: BALF, bronchoalveolar lavage fluid; TNF-α, tumor necrosis factor-a; IL1β, interleukin 1β; IL6, interleukin 6; HYP, hydroxyproline; COL-I, TypeIcollagen; FN, fibronectin.

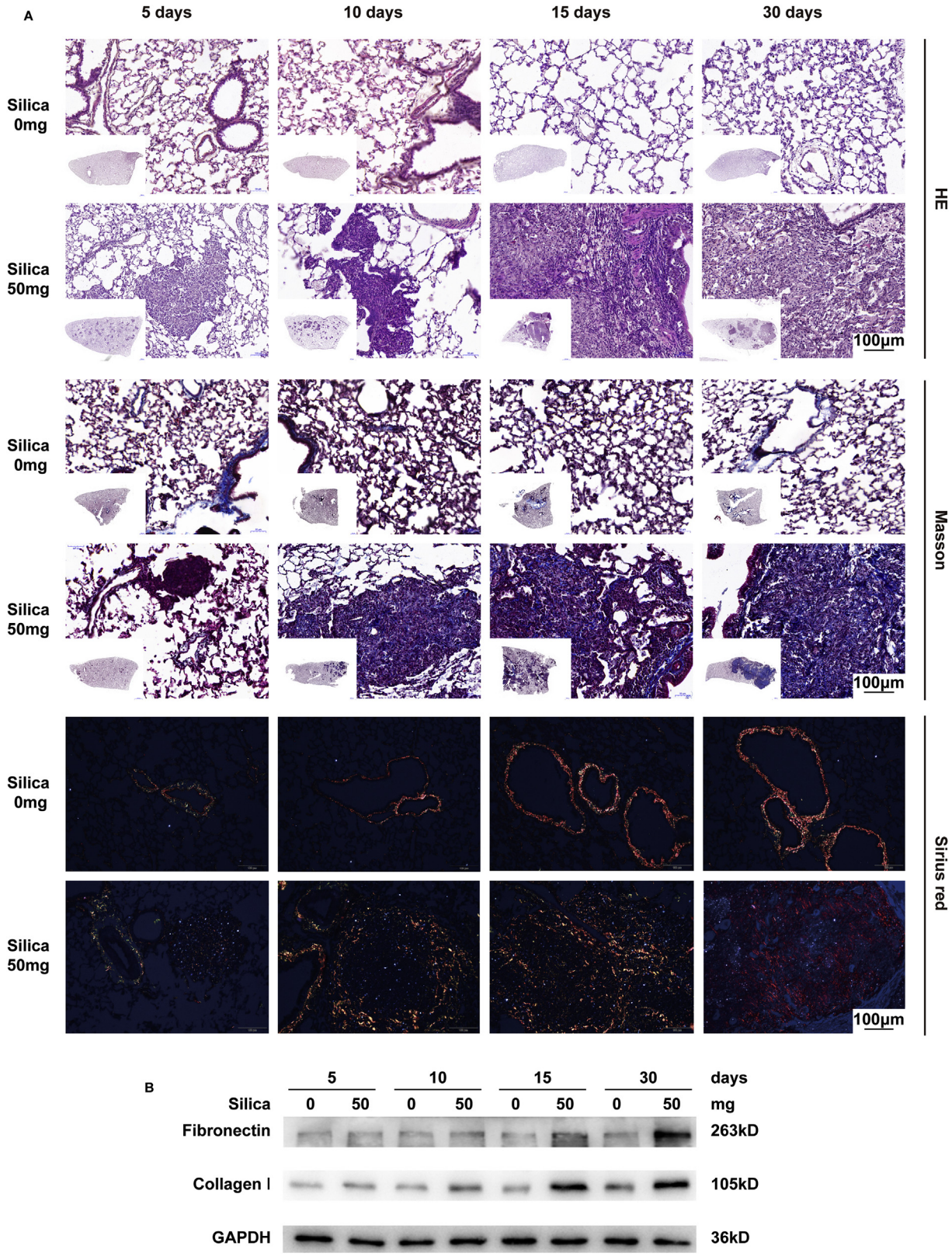


**Fig. 2.** Clarify the pathophysiological characteristics of silicosis in different rat models. Rats were exposed to silica of 0 mg (PBS, 1 mL) or 50 mg (50 mg/mL, 1 mL) for 5 days, 10 days, 15 days and 30 days respectively. A, Representative images of HE staining, Masson staining and Sirius red staining in lung tissues from different rat silicosis models (n = 5 for each group). B, Western blot showed the protein expression of collagen I and fibronectin in lung tissues from different rat silicosis models (n = 5 for each group). (For interpretation of the references to colour in this figure legend, the reader is referred to the Web version of this article.)

time (10–15 days) indicated by the decreased FVC and IC. Subsequently, a mixed ventilation disorder was shown in the late time (30 days), indicated by the decreased FEV300 and MMEF (Table 1). Moreover, with the increased of silica exposure time, silica instillation decreased lung quasi-static compliance (indicated by Cchord) but increased lung resistance (indicated by RI) (Table 1). Pulmonary hypertension induced by silica exposure can lead to an increase in right ventricular pressure and right ventricular hypertrophy (Omland et al., 2014). Similarly, our results also showed that silica exposure induced right ventricular hypertrophy in the early time (5–10 days), and increased pulmonary artery pressure in the late time (30 days), indicated by increased RVHI and RVSP (Table 1).

We next examined the pulmonary inflammation in rat models. As shown in Table 2 and Fig. 2A, the level of pulmonary inflammation started to ascend from day 5 and reached the highest level after day 15, indicated by increased Szapiel scores (calculated by HE staining), macrophage cell counts and inflammatory cytokines in BALF (Table 2). Differently, the development of pulmonary fibrosis was slower than inflammation. In details, the typical confluent silicotic nodule with central cavitation was observed at day 15, which resembled the typical pathological change in patients with advanced silicosis (Fig. 2A). And the severe fibrosis was observed at day 30 indicated by the up-regulated fibrotic markers (collagen I, fibronectin and HYP) (Table 2, Fig. 2B).

In summary, these results indicated that short time (5 days) exposure of silica could induce pulmonary inflammation, while longer time (15–30 days) exposure could cause significant pulmonary fibrosis and lung dysfunction in rats.

### 3.3. A novel classification reveals the pathophysiological progression of silicosis in rats

To further understand the pathophysiological process of silicosis in rats, we performed an unsupervised clustering analysis based on the alteration of important parameters including lung function, pulmonary inflammation and fibrosis in Tables 1 and 2. As shown in Fig. 3A, all samples were classified into four clusters. As expected, all the control (silica 0 mg) samples at different time points were grouped into “cluster 1” and other samples were grouped from “cluster 2” to “cluster 4” dependent on their different silica exposure time.

According to the different features of each cluster in rats, we defined the pathophysiological stages of silicosis as normal stage, inflammatory stage, progressive stage and fibrotic stage (Fig. 3B-Q). Specifically, 1) Normal stage (cluster 1) was the normal status without silica exposure. 2) Inflammatory stage (cluster 2) was the early stage of silicosis after 5 or 10 days of silica exposure and characterized by the up-regulated pulmonary inflammation, indicated by the increased parameters of Szapiel scores (Fig. 3F), the inflammatory cytokines (Figs. S1H–J) and the leukocytes in BALF (Fig. 3G–I). Additionally, slight pulmonary fibrosis (Fig. 3N–Q and S1K, L) and lung dysfunction (Fig. 3B, D, E and S1B) were also observed in this stage, which was consistent with the early stage of silicosis (Omland et al., 2014). 3) Progressive stage (cluster 3) was the middle stage with 15 days of silica exposure and featured by the progressive lung function impairment (Figs. 3B-E and S1A-E). Specifically, parameters of restrictive ventilatory disorder (IC and FVC) and lung compliance (Cchord) was significantly decreased compared to the normal stage (Fig. 3B, D, E). What's more, lung resistance (RI) was also dramatically increased in this stage (Fig. 3C). More importantly, MMEF started to aggravate in this stage, suggesting an obstructive ventilatory disorder and seriously damaged lung function (Fig. S1C). Additionally, pulmonary inflammation and fibrosis continued to deteriorate in this stage (Fig. 3G-L and N-Q). 4) Fibrotic stage (cluster 4) was the last stage of silicosis after 30 days of silica exposure and marked by severe pulmonary fibrosis. In details, Sirius red staining showed that collagen fibers surrounded the cavity of depositing birefringent particles (white) in the center of silicotic nodules (Fig. 2A), which resembled the typical silicotic nodules in human (Fig. 1A). Moreover, Masson staining presented similar distribution of collagen fibers (Blue) (Fig. 2A). Consistently, the fibrotic scores evaluated by Masson staining, the expression of HYP, collagen I and fibronectin were also dramatically up-regulated in this stage (Fig. 3O–Q and S1L). Furthermore, Cchord, FVC and FEV300 (Fig. 3D, E and S1E) were decreased compared with the progressive stage, suggesting the lung dysfunction deteriorated in this stage.

Taken together, we clarify the pathophysiological characteristics of silicosis in rat models and defined the process as four stages for the first time by using a new analysis method.

### 3.4. Clarify the pathophysiological characteristics of silicosis in different mouse models

Considering the importance of mouse models in the study of silicosis, we next constructed different mouse silicosis models and explored their pathophysiological characteristics. Similar to rats, mice also revealed lung dysfunction, pulmonary inflammation and fibrosis during the development of silicosis. However, several traits were observed in mouse remodels. Firstly, silica-induced lung dysfunction and right ventricle dysfunction in mice were more dependent on exposure doses than time. As shown in Supplementary Material Table 1, middle to high doses (12 mg and 16 mg) of silica were able to induce the lung function impairments (Ers, Rrs and G), pulmonary hypertension (RVSP) and right ventricular hypertrophy (RVHI) only after 3 weeks of exposure. However, lower doses (4 mg and 8 mg) of silica were not sufficient to induce these alterations even with longer exposure time (6 weeks and 9 weeks) (Table S1). Secondly, lung inflammation was found in early time (3 weeks) with higher doses (8 mg and 16 mg) of silica treatment. For example, exposure of 8 mg silica for 3 weeks could significantly up-regulate the cell number of macrophages and lymphocytes, and the concentration of inflammatory cytokines (TNF-α, IL-1β, IL-6) in BALF (Table S2). Similarly, HE staining (Fig. 4A) and Szapiel scores (Table S2) also showed obviously pulmonary inflammation. Finally, pulmonary fibrosis was only observed in mice treated with high dose (12 mg and 16 mg) of silica with longer exposure time (6 weeks and 9 weeks). For instance, exposure of 12 mg silica for 6 weeks or 16 mg for 9 weeks could result in a dramatic increase of fibrosis markers (Table S3, Fig. 4A and B). However, low and medium doses of silica (4 mg, 8 mg and 12 mg) were difficult to cause pulmonary fibrosis in a short exposure time (3 weeks).

Together, in mouse silicosis models, exposure with high doses (12 mg) of silica for a long time (6 weeks) were most efficient to induce lung function impairment, right ventricular dysfunction and pulmonary fibrosis. However, lower dose (4 mg and 8 mg) of silica was sufficient to initiate the inflammatory response in a short time (3 weeks).

### 3.5. Identify the silicosis progression in mouse models by the new classification method

To explore the pathophysiological characteristics of silicosis in mice, we performed the same analysis in mouse silicosis models. Consistent to the results in rats, four clusters (cluster 1–4) were exhibited during the progression of silicosis in mice. As shown in Fig. 5A, all the control (0 mg) samples as well as the 4 mg_3w samples were included in “cluster 1”. The “cluster 2” mainly grouped with 4 mg_3w, 4 mg_6w and 4 mg_9w. Mice with high doses (12 mg and 16 mg) at short time (3 weeks) or intermediate dose (8 mg) at short and intermediate exposure time (3 weeks and 6 weeks) were mainly included in “cluster 3”. While most samples with higher dose and longer exposure time were belonging to “cluster 4” , including 8 mg_9w, 12 mg_6w, 12 mg_9w, 16 mg_6w, 16 mg_9w.

Based on the pathophysiological features of the four clusters, we defined the progression of silicosis in mice as normal stage (cluster 1), inflammatory stage (cluster 2), progressive stage (cluster 3) and fibrotic stage (cluster 4). 1) Normal stage, all the control (0 mg) samples as well

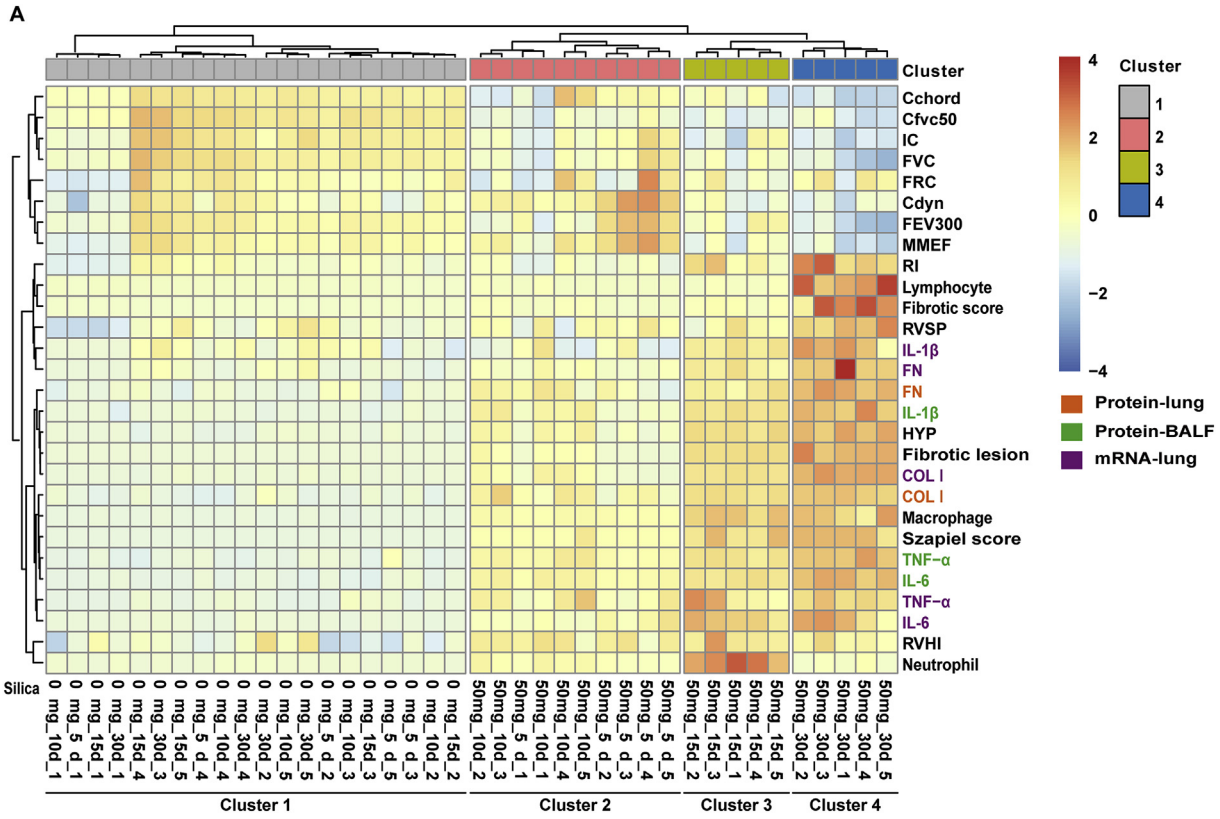


**Fig. 3.** A novel classification reveals the pathophysiological progression of silicosis in rats. A, Hierarchical cluster heat map of rats showed the pathophysiological characteristics of lung function, right ventricle function, pulmonary inflammation and pulmonary fibrosis in each cluster. B, C, D and E, Statistical diagrams of rat lung function included IC (B), RI (C), Cchord (D), and FVC (E) in each cluster. F, The inflammatory scores of HE staining images of lung tissues were evaluated by Szapiel's method in each cluster. G, H and I, The cell counts of macrophage (G), neutrophil (H) and lymphocyte (I) in BALF from each cluster. J, K and L, The mRNA expression of inflammatory cytokines included TNF-α (J), IL-1β (K), and IL-6 (L) in lung tissues from each cluster. M, The fibrotic scores of Masson staining images from rat lung tissues in each cluster. N, The positive area of fibrotic lesions by Sirius red staining from rat lung tissues in each cluster. O, Hydroxyproline contents from rat lung tissues in each cluster. P and Q, The mRNA expression of collagen I (P) and fibronectin (Q) in each cluster. For all statistical plots, the data are presented as the mean ± SD; $*P < 0.05$; $**P < 0.01$. Abbreviations: IC, inspiratory capacity; RI, lung resistance; Cchord, chord compliance; FVC, forced vital capacity. (For interpretation of the references to colour in this figure legend, the reader is referred to the Web version of this article.)

as the 4 mg_3w samples were included, indicating that exposure to the low dose and short duration did not show pathophysiological alteration. 2) Inflammatory stage was characterized by significantly increased pulmonary inflammation in the lung. Several inflammation-related parameters were significantly up-regulated in this stage, such as the cell counts of lymphocytes in BALF (Fig. S2G), the expression of inflammatory cytokines (IL-6, IL-1β, and TNF-α) in BALF and lung tissues (Fig. 5H–J, and S2H-J). 3) Progressive stage showed an significant impairment of lung function (Figs. 5B-F, and S2A-D) as well as deteriorated pulmonary inflammation and fibrosis. In details, Cst and Crs (Fig. 5B, E) were significantly decreased, while Rrs, G, and Ers were increased in this stage (Fig. 5C, D, F). Moreover, inflammatory cytokines and leukocytes in BALF also continued to increase in this stage (Fig. 5H–J and S2E-G). 4) Fibrotic stage revealed the severe pulmonary fibrosis. Specifically, typical silicotic nodules reveled by Masson staining and Sirius red staining (Fig. 4A) were similar to chronic silicosis lesions in human (Fig. 1A). In these nodules, the cavity center of deposited silica particles was surrounded by collagen fibers and dust-laden macrophages. In addition, the expression of fibrotic markers including fibrotic scores, positive fibrotic lesion, HYP, collagen I and fibronectin were also reached the highest level in this stage (Fig. 5K-P).

Taken together, through the novel pathophysiological classification, we defined the progression of silicosis in mice as normal stage, inflammatory stage, progressive stage and fibrotic stage and clarify the pathophysiological features of each stage.

## 4. Discussion

In this study, using unsupervised clustering analysis, we defined the pathophysiological process of silicosis as four stages: normal stage, inflammatory stage, progressive stage and fibrotic stage in both rat and mouse models, and the common features were found in each stage. Specifically, pulmonary inflammation worsened dramatically during the inflammatory stage (stage 2), and maintained at high level until fibrotic stage (stage 4). Lung dysfunction was mainly manifested in the progressive stage (stage 3) and further deteriorated at the fibrotic stage (stage 4). What's more, significant pulmonary fibrosis mainly appeared at the fibrotic stage (stage 4), and only mild fibrosis was found in the inflammatory stage (stage 2) and progressive stage (stage 3). In addition, our results suggested the possible protocols (dose and time of silica exposure in tracheal instillation) to establish silicosis models in different stages.

In the progression of silicosis, the relationship between lung dysfunction and pulmonary inflammation and fibrosis is still unclear. Here, our results (Fig. 3G–J, L, 5H-J, and S1H-J, S2G-J) showed that silica exposure mainly induced remarkably pulmonary inflammation in the early stage (inflammatory stage) of silicosis. However, no significant lung dysfunction and pulmonary fibrosis were appeared in this stage, indicating that acute pulmonary inflammation does not significantly affect lung function. Subsequently, with the aggravation of pulmonary inflammation (Fig. 3G-L, 5H-J), pulmonary fibrosis (Fig. 3N–Q, 5K, M, O, P, S1K, L) worsened significantly in progressive stage. More

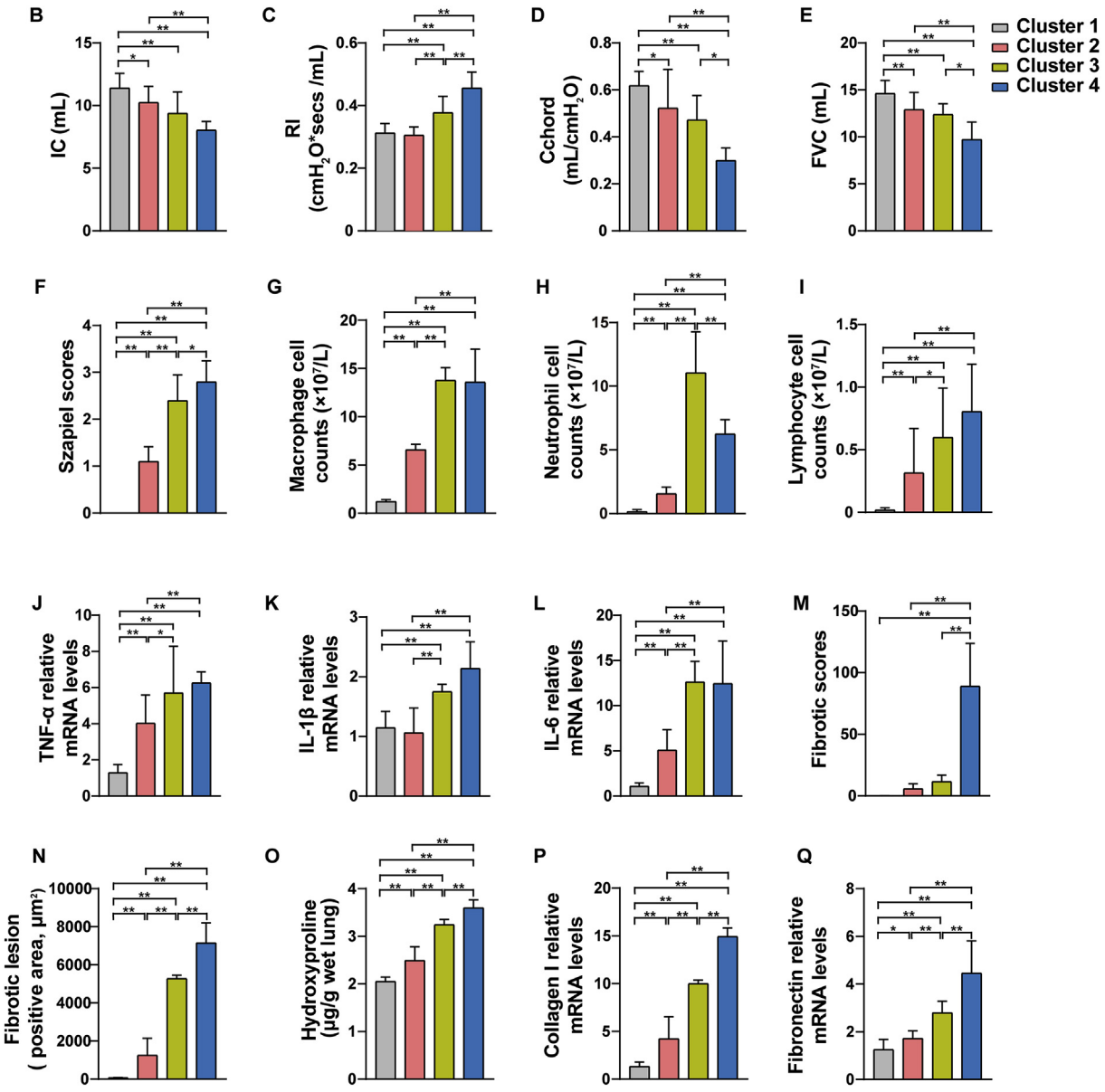


**Fig. 3.** (*continued*)

importantly, lung dysfunction including aberrant lung resistance and compliance (Fig. 3C–E, 5 B–F, S1A, C) were also appeared in progressive stage and continued to deteriorate with the aggravation of pulmonary fibrosis in fibrotic stage. These observations suggest that the aggravation of pulmonary fibrosis induced by persistent pulmonary inflammation may be the leading cause of lung dysfunction in silicosis.

In the present study, some common features were founded in silicosis patients and rodents. In normal stage (stage 1), the histological staining of lung in both human and rodents showed clear alveolar structure and no exudate in the alveolar cavity (Figs. 1A, 2A and 4A). In fibrotic stage (stage 4), severe pulmonary fibrosis were appeared (Figs. 1A, 2A and 4A), including a thickened alveolar wall with a certain amount of cellulose forming cell clusters and silicon nodules in the alveolar matrix. Moreover, several parameters of pulmonary inflammation and fibrosis (Fig. 1B, C, D, 3G-Q, 5H-Q) were also significantly increased in both silicosis patients and rodents. Collectively, the similar pathophysiological features that we observed in rodents and humans suggest that the pathophysiological processes shown in the silicosis models may also exist in silicosis patients, which needs to be further confirmed.

In this study, unsupervised clustering analysis (Figs. 3A and 5A) could provide some reliable suggestions for the construction of silicosis models at different stages. In details, silica exposure at 4 mg for 6 weeks in mice and 50 mg for 5 days or 10 days in rats might be appropriate conditions to induce silicosis in inflammatory stage. For progressive stage, 12 mg of silica for 3 weeks, 8 mg of silica for 6 weeks in mice and 50 mg of silica for 15 days in rats may be a good choice. To construct fibrotic stage, exposure to silica at 8 mg for 9 weeks or 12 mg for 6 weeks in mice or 50 mg of silica for 30 days in rats are suitable.

There were some limitations in this study. Firstly, restricted parameters were used for the unsupervised clustering analysis. More worthwhile markers need to be added in the future study, such as TGF-β that was also increased in the lung tissue of silicosis (Zhang et al., 2019). Secondly, the number of rodents in each group is limited due to the experimental conditions. More samples will be better. In summary, we defined the pathophysiological process of silicosis as four stages: normal stage, inflammatory stage, progressive stage and fibrotic stage and characterized the pathophysiological features during the progression of silicosis. Our results also provided some suggestions about the construction of silicosis models in different stages and maybe helpful

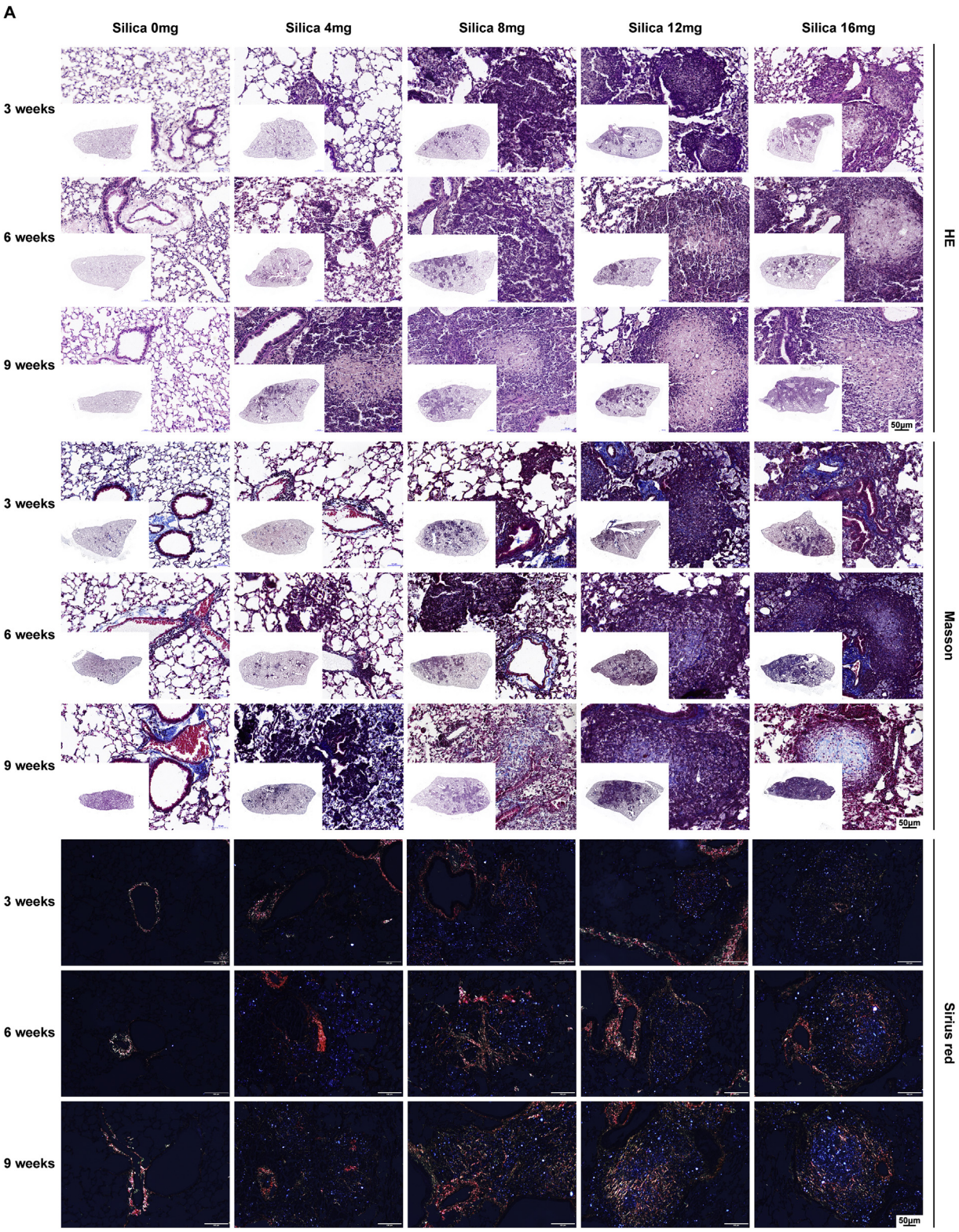


**Fig. 4.** Clarify the pathophysiological characteristics of silicosis in different mouse models. Mice were exposed to silica at different doses (4 mg, 8 mg, 12 mg, and 16 mg) and time (3 weeks, 6 weeks and 9 weeks) respectively. A, Representative images of HE staining, Masson staining and Sirius red staining in lung tissues from different mouse silicosis models (n = 5 for each group). B, The expression of collagen I and fibronectin in lung tissues from different models were detected by Western blot (n = 5 for each group). (For interpretation of the references to colour in this figure legend, the reader is referred to the Web version of this article.)

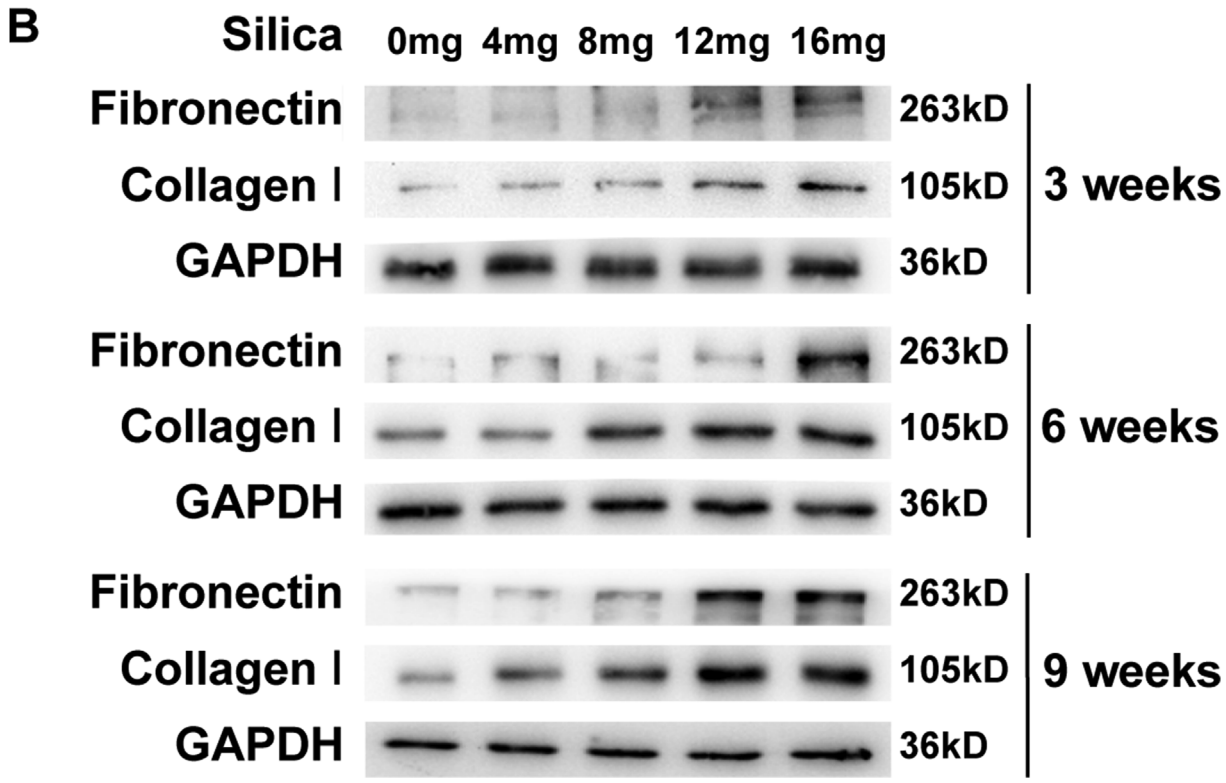


**Fig. 4.** (*continued*)

for the further exploration of molecular mechanisms or therapeutic targets of this disease.

## CRediT authorship contribution statement

**Zhujie Cao:** Methodology, Data curation, Writing - original draft. **Meiyue Song:** Writing - original draft, Methodology, Data curation. **Ying Liu:** Writing - original draft, Methodology, Data curation. **Junling Pang:** Formal analysis. **Zhaoguo Li:** Methodology. **Xianmei Qi:** Methodology. **Ting Shu:** Methodology. **Baicun Li:** Resources. **Dong Wei:** Resources. **Jingyu Chen:** Resources. **Bolun Li:** Writing - original draft. **Jing Wang:** Methodology, Writing - review & editing, Supervision. **Chen Wang:** Methodology, Writing - review & editing, Supervision.

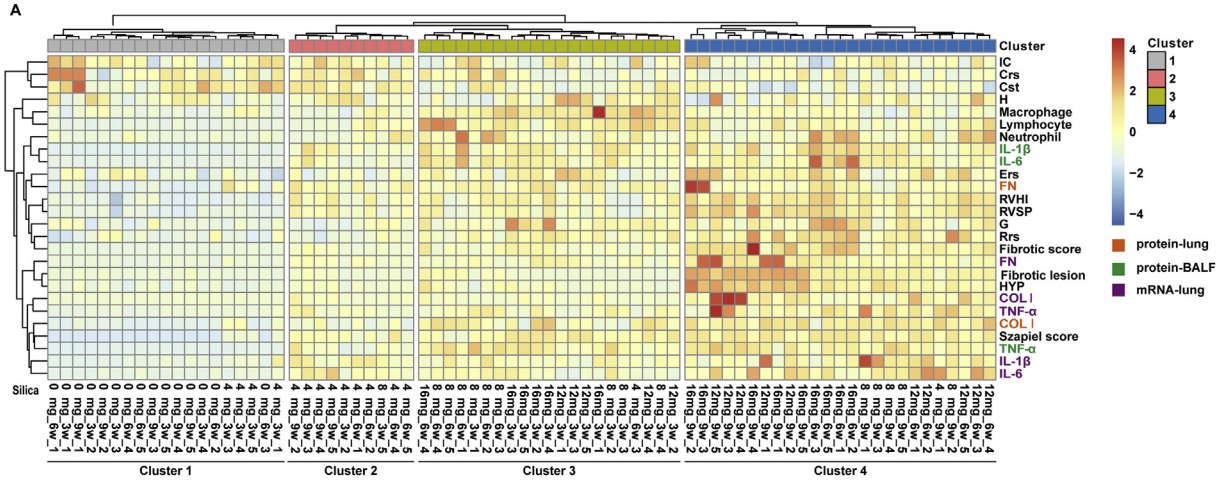


**Fig. 5.** Identify the silicosis progression in mouse models by the new classification method. A, Hierarchical cluster heat map of mouse showed the pathophysiological characteristics of lung function, right ventricle function, pulmonary inflammation and pulmonary fibrosis in each cluster. B, C, D, E and F, Statistical diagrams of mouse lung function included Cst (B), Rrs (C), Ers (D), Crs (E) and G (F) in each cluster. G, The inflammatory scores of HE staining images of lung tissues were evaluated by Szapiel's method in each cluster. H, I and J, The expression of inflammatory cytokines in BALF of each cluster. K, The fibrotic scores of Masson staining images of mouse lung tissues in each cluster. L, The positive area of Sirius red staining from mouse lung tissues in each cluster. M, Hydroxyproline contents from mouse lung tissues in each cluster. N, O, P and Q, The expression of collagen I (N, O) and fibronectin (P, Q) in both mRNA and protein levels from each cluster. For all statistical plots, the data are presented as the mean ± SD; $*P < 0.05$; $**P < 0.01$. Abbreviations: Cst, quasi-static compliance; Rrs, resistance of respiratory system; Ers, elastance respiratory of system; Crs, dynamic compliance; G, tissue damping. (For interpretation of the references to colour in this figure legend, the reader is referred to the Web version of this article.)

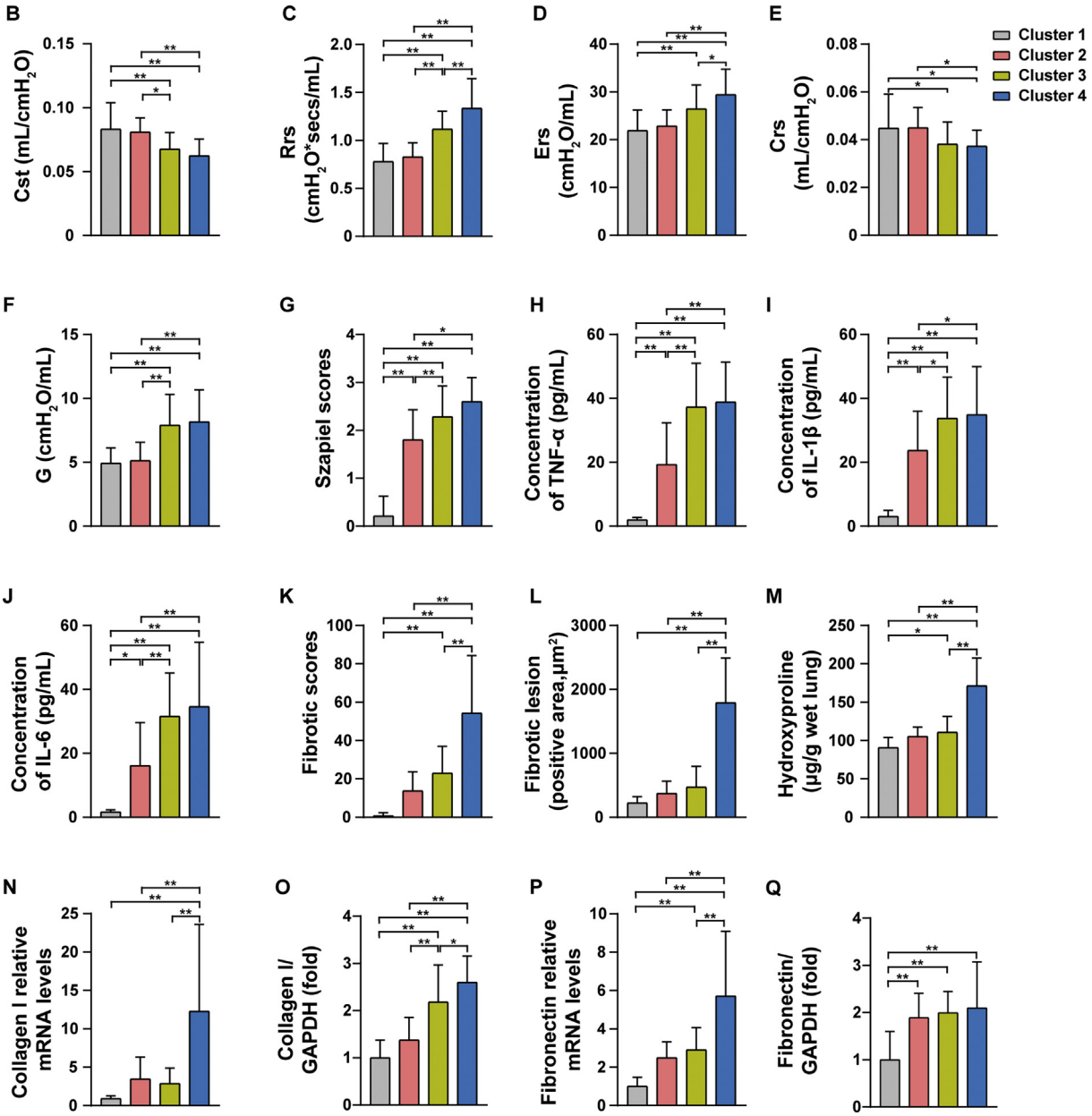


**Fig. 5.** (*continued*)

## Declaration of competing interest

The authors declare that they have no known competing financial interests or personal relationships that could have appeared to influence the work reported in this paper.

## Acknowledgments

This work was financially supported by Chinese Academy of Medical Sciences Innovation Fund for Medical Sciences [grant number: 2018–I2M-1-001] (to C.W.), the National Natural Science Foundation of China [grant numbers: 81622008, 91739107] (to J.W.), Thousand Young Talents Program of China (to J.W.).

## Appendix A. Supplementary data

Supplementary data to this article can be found online at https://doi.org/10.1016/j.ecoenv.2020.110834.

## References

Beamer, C.A., Migliaccio, C.T., Jessop, F., Trapkus, M., Yuan, D., Holian, A., 2010. Innate immune processes are sufficient for driving silicosis in mice. J. Leukoc. Biol. 88, 547–557. https://doi.org/10.1189/jlb.0210108.

Cohen, R.A., et al., 2016. Lung pathology in U.S. Coal workers with rapidly progressive pneumoconiosis implicates silica and silicates. Am. J. Respir. Crit. Care Med. 193, 673–680. https://doi.org/10.1164/rccm.201505-1014OC.

Cruz, F.F., et al., 2016. Dasatinib reduces lung inflammation and fibrosis in acute experimental silicosis. PloS One 11, e0147005. https://doi.org/10.1371/journal.pone.0147005.

Devos, F.C., et al., 2017. Forced expiration measurements in mouse models of obstructive and restrictive lung diseases. Respir. Res. 18, 123. https://doi.org/10.1186/s12931-017-0610-1.

Du, S., et al., 2019. Dioscin alleviates crystalline silica-induced pulmonary inflammation and fibrosis through promoting alveolar macrophage autophagy. Theranostics 9, 1878–1892. https://doi.org/10.7150/thno.29682.

Ehrlich, R., Murray, J., Rees, D., 2018. Subradiological silicosis. Am. J. Ind. Med. 61, 877–885. https://doi.org/10.1002/ajim.22909.

Feng, F., et al., 2020. Tanshinone IIA attenuates silica-induced pulmonary fibrosis via inhibition of TGF-β1-Smad signaling pathway. Biomed. Pharmacother. 121, 109586. https://doi.org/10.1016/j.biopha.2019.109586.

Fernández, Á.R., Martínez, G.C., Quero, M.A., Blanco, P.J.J., Carazo, F.L., Prieto, F.A., 2015. Guidelines for the diagnosis and monitoring of silicosis. Arch. Bronconeumol.

51, 86–93. https://doi.org/10.1016/j.arbres.2014.07.010.
Fröhlich, E., Salar-Behzadi, S., 2014. Toxicological assessment of inhaled nanoparticles: role of in vivo, ex vivo, in vitro, and in silico studies. Int. J. Mol. Sci. 15, 4795–4822. https://doi.org/10.3390/ijms15034795.
Fujimura, N., 2000. Pathology and pathophysiology of pneumoconiosis. Curr. Opin. Pulm. Med. 6, 140–144. https://doi.org/10.1097/00063198-200003000-00010.
Guo, J., Yang, Z., Jia, Q., Bo, C., Shao, H., Zhang, Z., 2019. Pirfenidone inhibits epithelial-mesenchymal transition and pulmonary fibrosis in the rat silicosis model. Toxicol. Lett. 300, 59–66. https://doi.org/10.1016/j.toxlet.2018.10.019.
James, S.L., Abate, D., et al., 2018. Global, regional, and national incidence, prevalence, and years lived with disability for 354 diseases and injuries for 195 countries and territories, 1990-2017: a systematic analysis for the Global Burden of Disease Study 2017. Lancet 392, 1789–1858. https://doi.org/10.1016/S0140-6736(18)32279-7.
Joubert, K.D., et al., 2019. Outcomes after lung transplantation for patients with occupational lung diseases. Clin. Transplant. 33, e13460. https://doi.org/10.1111/ctr.13460.
Karkale, S., Khurana, A., Saifi, M.A., Godugu, C., Talla, V., 2018. Oropharyngeal administration of silica in Swiss mice: a robust and reproducible model of occupational pulmonary fibrosis. Pulm. Pharmacol. Therapeut. 51, 32–40. https://doi.org/10.1016/j.pupt.2018.06.003.
Kato, K., Zemskova, M.A., Hanss, A.D., Kim, M.M., Summer, R., Kim, K.C., 2017. Muc1 deficiency exacerbates pulmonary fibrosis in a mouse model of silicosis. Biochem. Biophys. Res. Commun. 493, 1230–1235. https://doi.org/10.1016/j.bbrc.2017.09.047.
Leung, C.C., Yu, I.T., Chen, W., 2012. Silicosis. Lancet. 379 (9830), 2008–2018.
Mayeux, J.M., Kono, D.H., Pollard, K.M., 2019. Development of experimental silicosis in inbred and outbred mice depends on instillation volume. Sci. Rep. 9, 14190. https://doi.org/10.1038/s41598-019-50725-9.
Muszyńska-Graca, M., Dąbkowska, B., Brewczyński, P.Z., 2016. [Guidelines for the use of the international classification of radiographs of pneumoconioses of the international labour office (ILO): substantial changes in the currrent edition]. Med. Pr. 67, 833–837. https://doi.org/10.13075/mp.5893.00493.
Omland, O., Würtz, E.T., Aasen, T.B., et al., 2014. Occupational chronic obstructive pulmonary disease: a systematic literature review. Scand. J. Work. Environ. Health 40 (1), 19–35.
Sun, J., et al., 2019. MicroRNA-29b mediates lung mesenchymal-epithelial transition and prevents lung fibrosis in the silicosis model. Mol. Ther. Nucleic Acids 14, 20–31. https://doi.org/10.1016/j.omtn.2018.10.017.
Vanhée, D., Gosset, P., Boitelle, A., Wallaert, B., Tonnel, A.B., 1995. Cytokines and cytokine network in silicosis and coal workers' pneumoconiosis. Eur. Respir. J. 8, 834–842.
Yan, W., et al., 2016. SB203580 inhibits epithelial-mesenchymal transition and pulmonary fibrosis in a rat silicosis model. Toxicol. Lett. 259, 28–34. https://doi.org/10.1016/j.toxlet.2016.07.591.
Zhai, R., Ge, X., Li, H., Tang, Z., Liao, R., Kleinjans, J., 2004. Differences in cellular and inflammatory cytokine profiles in the bronchoalveolar lavage fluid in bagassosis and silicosis. Am. J. Ind. Med. 46, 338–344. https://doi.org/10.1002/ajim.20051.
Zhang, E., et al., 2018. Bone marrow mesenchymal stromal cells attenuate silica-induced pulmonary fibrosis potentially by attenuating Wnt/β-catenin signaling in rats. Stem Cell Res. Ther. 9, 311. https://doi.org/10.1186/s13287-018-1045-4.
Zhang, Z.Q., Shao, B., Han, G.Z., Liu, G.Y., Zhang, C.Z., Lin, L., 2019. Location and dynamic changes of inflammation, fibrosis, and expression levels of related genes in SiO2-induced pulmonary fibrosis in rats in vivo. J. Toxicol. Pathol. 32, 253–260. https://doi.org/10.1293/tox.2019-0024.
Zhao, Y., et al., 2020. Silica particles disorganize the polarization of pulmonary macrophages in mice. Ecotoxicol. Environ. Saf. 193, 110364. https://doi.org/10.1016/j.ecoenv.2020.110364.